Computational Chemistry-based identification of Ultra-Low Temperature Water-Gas-Shift Catalysts

Final Technical Report
September 1, 2006 - June 30, 2008

Professor Manos Mavrikakis

June 2008

Department of Chemical and Biological Engineering
University of Wisconsin - Madison
Madison, WI 53706

Disclaimer

Abstract

The current work seeks to identify novel, catalytically-active, stable, poison-resistant LWGS catalysts that retain the superior activity typical of conventional Cu catalysts but can be operated at similar or lower temperatures. A database for the Binding Energies (BEs) of the LWGS relevant species, namely CO, O and OH on the most-stable, close-packed facets of a set of 17 catalytically relevant transition metals was established. This BE data and a database of previously established segregation energies was utilized to predict the stability of bimetallic NSAs that could be synthesized by combinations of the 17 parent transition metals. NSAs that were potentially stable both *in vacuo* and under the influence of strong-binding WGS intermediates were then selected for adsorption studies. A set of 40 NSAs were identified that satisfied all three screener criteria and the binding energies of CO, O and OH were calculated on a set of 66, 43 and 79 NSA candidates respectively. Several NSAs were found that bound intermediates weaker than the monometallic catalysts and were thus potentially poison-resistant. Finally, kinetic studies were performed and resulted in the discovery of a specific NSA-based bimetallic catalyst Cu/Pt that is potentially a promising LWGS catalyst. This stable Cu/Pt sub-surface alloy is expected to provide facile H_2O activation and remain relatively resistant from the poisoning by CO, S and formate intermediates.

Table of Contents

Executive Summary

The Low Temperature Water Gas Shift (LWGS) Reaction (CO+H_2O$\rightarrow$ CO_2 + H_2) is an industrially important reaction because of its key role in the production and purification of H_2 for various applications. In addition to its application for H_2 production and purification from fossil-fuels, LWGS is also employed in fuel cells to remove any residual CO impurity which has potential to severely interfere with fuel cell operation. The exothermic nature of the WGS reaction necessitates operation at relatively low temperatures in order to obtain a favorable equilibrium distribution that maximizes the desired products (CO_2 +H_2). The low-temperature operation, unfortunately, causes a concomitant penalty on the reaction rates that might be achieved by conventional catalysts. Cu is the typical catalyst employed for most industrial applications of LWGS, yet there exists considerable incentive for the discovery of novel, poison-resistant, LWGS catalysts that demonstrate long-term stability, and provide activity improvement over Cu and yet are able to operate at similar or lower temperatures. In spite of its long history as a LWGS catalyst the fundamental reaction mechanisms for LWGS on Cu and other transition metals are still the subject of considerable debate and hence our first-principles based calculations can help in providing the insights required for truly rational LWGS catalyst design.

Our first-principles studies tried to identify stable, poison-resistant, bimetallic Near Surface Alloys (NSAs) that would be potentially suitable LWGS Catalysts. We restricted our studies to alloys made from a set of 17 catalytically relevant Transition Metals. Although bimetallic alloys can exist in a variety of configurations NSAs were the only class studied in this project. NSAs are alloys with a solute metal near the surface of a host metal at concentrations different from those in the bulk. Numerous recent studies have attributed NSAs with novel electronic and catalytic properties (for hydrogen storage applications and fuel cell electrodes) considerably distinct from the parent metals that they are constituted from. In addition NSAs can be synthesized at compositions that would not be deemed to be thermodynamically stable for conventional bulk alloys. Previous work on Cu had identified the ease of H_2O activation along with the strength of OH, CO and O binding as reasonable descriptors of WGS activity and hence our studies started with calculations for the adsorption of these adsorbates on the set of 17 transition metals. All high-symmetry sites on the close packed facets of each transition metal were considered and the binding energies (BEs) and site-preferences were evaluated. Calculations for Sulfur adsorption were also undertaken in view of the fact that Sulfur is one of the most relevant poisons that negatively affects the activity of WGS catalysts.

We found that the noble metals tend to bind the adsorbates weaker than the rest and for the adsorption of CO in particular there is a distinct "BE-gap" between the binding strength of adsorbates on the noble metals and the others. Cu, the conventional LWGS catalyst exhibits a very low BE_{CO}. After having established this database for the BE of adsorbates on noble metals we proceeded to calculations on bimetallic NSAs. The primary criterion we applied was the long-term stability of these NSAs *in vacuo* and in presence of adsorbates likely to be in the ambient of LWGS processing. A set of

5

"screener-plots" were constructed by utilizing the BE data for adsorbates on the monometallic systems and a previous database of segregation energies. In the interest of computational feasibility this set was further pruned by applying heuristics based on past experience and the BEs for CO, O and OH were established on a 66, 43 and 79 NSA candidates respectively. 40 NSAs were found that satisfied the criteria of surviving all three screeners. Both overlayer and sub-surface alloy type NSAs were considered and a database of CO, O and OH BEs was established. This database serves as a fertile source to apply data-mining approaches for rational catalyst design as a part of this and future studies. Several NSAs were discovered that bind adsorbates weaker than any of the monometallic systems studied so far e.g. Au*/Ir, and Pt*/Cu for O and Pt*/Cu for OH. In addition some NSAs display an interesting behavior since they bind adsorbates with a strength that is weaker than what we would expect on the basis of either parent-metal e.g. Au*/Re binds O weaker than both Au and Re. We discovered that the metal exposed on the surface of the NSA catalyst has the primary dominant influence on adsorbate BE in most cases whereas the underlying metal only has a weaker modulating influence. Further, we identified four NSAs that bind CO weaker than Cu and hence might prevent CO-poisoning of the LWGS catalyst.

In the last stage of the project we performed Minimum Energy Pathway (MEP) calculations using the climbing-image Nudged Elastic Band (NEB) method to evaluate the thermochemistry and kinetics for H_2O activation on a set of carefully selected promising WGS catalysts. Specifically, the elementary step $H_2O \rightarrow OH + H$ was analyzed since previous work has implicated this as a Rate Determining Step (RDS) on a variety of TMs including Cu. The most significant bimetallic alloy catalyst discovered was the Cu/Pt system which provides facile H_2O activation yet binds the products (OH + H) weaker than Cu. This catalyst was shown to be significantly resistant to poisoning by both CO and formate species by virtue of their weak adsorption. This Cu/Pt NSA shows an enhancement of Cu concentration in the first sub-surface of the Pt host and this system was demonstrated to be stable in CO-rich environments and thus resistant to CO-induced segregation and reconstruction. Finally, verification of the superior nature of the Cu/Pt catalyst was performed by XPS, TPD and STM techniques undertaken by our collaborating-researchers. Thus the major success of the project was the establishment of databases for the BEs of CO, O and OH on transition-metals and NSAs and further in utilizing this database (in conjunction with stability criteria) for the discovery of a novel-LWGS catalytic system, Cu/Pt.

1. Introduction

1.1. Motivation and Background

The Low Temperature Water Gas Shift (LWGS) Reaction (CO+$H_2O \rightarrow CO_2 + H_2$) is an industrially important reaction because of its key role in the production and purification of H_2 for various applications. Several dominant routes for H_2 production from fossil fuels incorporate the WGS reaction at some stage in their processing scheme, most commonly as a sequence at high temperature and low temperature conditions. Another important LWGS application is the purification of feed H_2 for low temperature fuel cells by removal of residual CO since most fuel cells mandate stringent limits on the CO concentrations they can tolerate. The WGS reaction is somewhat exothermic ($\Delta H_{298}^0 \sim -40 kJ/mol$) and hence must be operated at relatively low temperatures in order to drive the reaction equilibrium in favor of the desired products ($CO_2 + H_2$). In turn, low temperature places penalties on the reaction rates and that is why most large-scale industrial operations employ a high temperature WGS reactor followed by a LWGS reactor. For other applications with a space constraint, most notably automotive fuel-cells, such a two-stage scheme is not viable. Cu is currently the catalyst of choice for most LWGS applications and at the relatively low temperatures involved (<250° C) the native activity of Cu catalysts is low and imposes significant kinetic limitations on the process. Despite a number of experimental studies[1-3], the detailed LWGS reaction mechanism on various transition metals remains elusive, precluding truly rational catalyst improvements. As a result, significant incentives prevail for the identification of novel LWGS catalysts that provide activity improvements over Cu and yet are able to operate at similar or, even better, lower temperatures.

1.2. Overview of our Calculation Approach

The principal goal of our project is the identification of stable, bimetallic, Near Surface Alloy (NSA) based LWGS catalysts that satisfy the aforementioned dual

objectives of high-activity and low temperature operation. We employ a sate-of-the-art, first-principles approach based on periodic, self-consistent Density Functional Theory (DFT) to screen and select a set of potentially promising LWGS catalysts and subsequently obtain a detailed understanding of the LWGS reaction mechanism on these selected bimetallic alloys by means of detailed kinetic studies. Our study considers bimetallic formulations derived from a set of 17 catalytically relevant transition metals (Au, Ag, Cu, Pd, Pt, Ir, Ni, Co, Rh, Fe, Os, Ru, Re, Mo, W, Ta and V). A catalytically active nanoparticle would consist of several different crystal facets of these metals but the low-index, close-packed facets could be expected to dominate. Hence we focus on these, stable, low-energy facets of the transition metals and Near Surface Alloys under study.

Our study can be divided into several stages. Foremost we start with calculations for evaluating the binding energy (BE) for the intermediates of interest (O, OH and CO) on the close-packed facets of the 17 pure transition metals. The next stage involves the study of the stability of these alloys *in- vacuo* and also in the presence of the relevant adsorbed intermediates. The BEs on pure metals and knowledge of the segregation energies of the transition metals allows us to construct "screener plots" for each of these adsorbates. Based on these plots we identify bimetallic combinations that might be stable yet active. This then leads to the next stage wherein we perform calculations to evaluate the BEs for these adsorbates on a set of promising NSAs. Finally we focus on a small number of NSAs and perform kinetic calculations on these for H_2O activation, typically the most difficult step in WGS. Finally, *Sulfur* is a common poison for these catalysts and hence the binding of Sulfur was also studied on several of these alloys to probe their resistance to Sulfur poisoning. In the following sections we try to summarize the results of these calculations.

2. **Theoretical Methods**

All calculations are performed using the total energy code DACAPO[4,5]. Adsorption is allowed on only one of the two surfaces of the slab and the electrostatic potential is adjusted accordingly. Calculations are performed spin-polarized where necessary (e.g.: metals or alloys including: Fe, Co, or Ni). We use a 2x2x4 unit cell with 5 equivalent layers of vacuum in between successive slabs and relax the top two layers of the slabs. The Kohn-Sham one-electron valence states are expanded in a basis of plane waves with a kinetic energy below 25 Ry. The exchange-correlation energy and potential are described by the generalized gradient approximation (GGA-PW91); the ionic cores are described by ultrasoft pseudopotentials. The surface Brillouin zone is sampled with a *4x4x1 Monkhorst-Pack* or a *Chadi-Cohen* k point set, as appropriate.

3. **Results and Discussion**

## 3.1. Adsorption of CO, O and OH on monometallic facets

In the first part of the project we performed calculations for the adsorption of CO, O and OH on the closed packed facets of all 17 transition metals under investigation. The spectrum plot (Figure 1) shows the magnitude of BE's for CO. We found that BE_{CO} spans a range of about 2.4 eV with Ag binding the weakest (-0.3 eV) and V the strongest (-2.69 eV). The noble metals Ag, Au and Cu form a group of weak binding metals and every other metal binds CO stronger than these; in fact these three metals have a substantially superior performance than the rest and a BE_{CO} "gap" of about 1 eV separates this group from the other metals. Previous DFT studies in our group had identified the strength of CO binding as one of the two main descriptors characterizing WGS activity (the other being the ease of H_2O activation). Cu performs well for LWGS due to a combination of a medium strength of CO binding and a rather facile H_2O activation; our goal was to find NSAs that could bridge (or even better, transcend) the gap around Cu on this spectrum plot, while retaining the ability to perform facile H_2O activation.
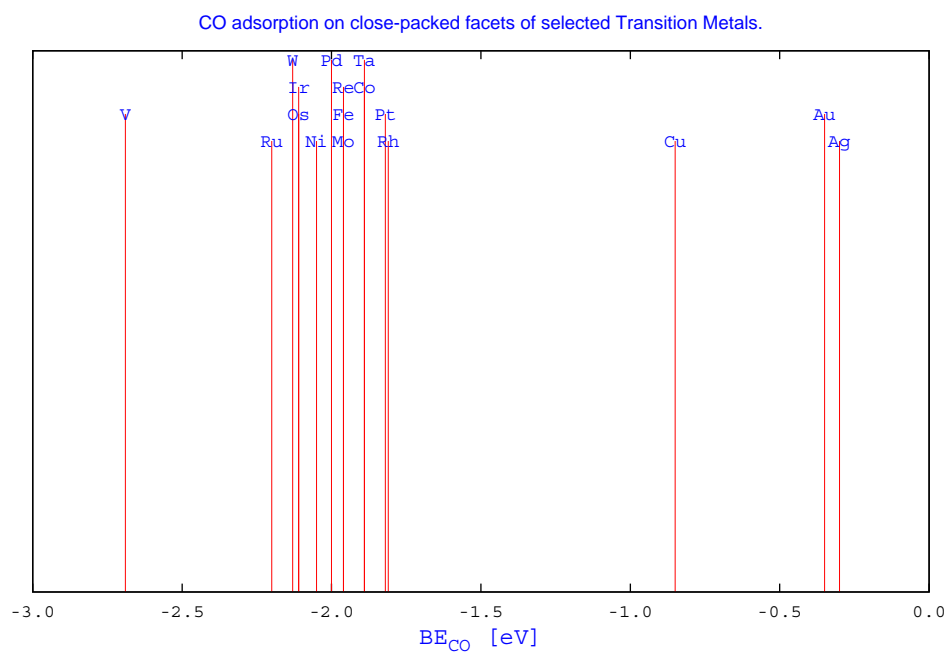
Figure 1 Strength of CO binding on monometallic transition-metal surfaces.
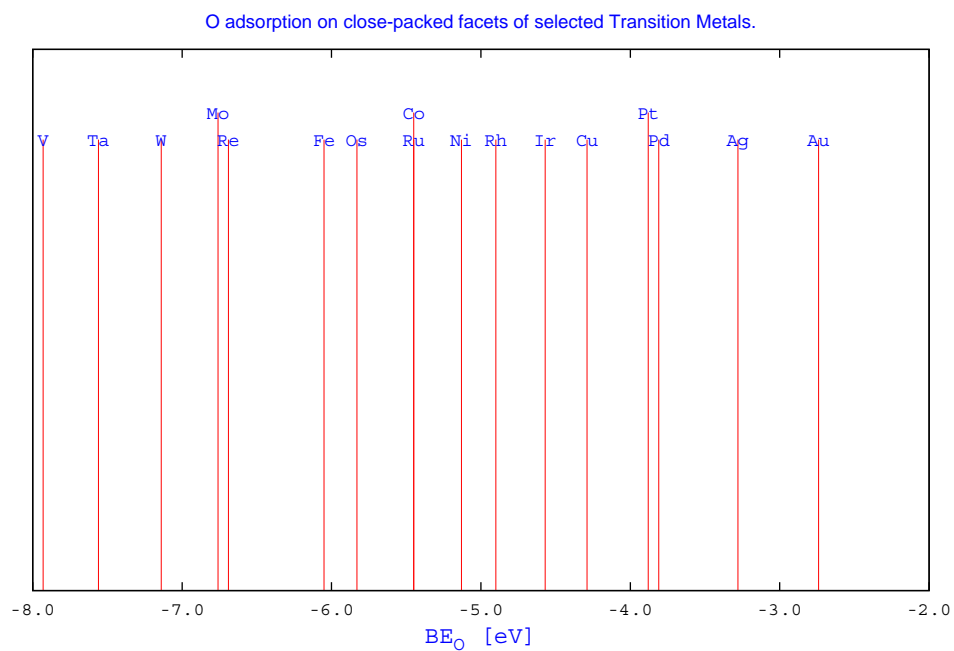
Figure 2 Strength of O binding on monometallic transition-metal surfaces.

OH adsorption on close-packed facets of selected Transition Metals.
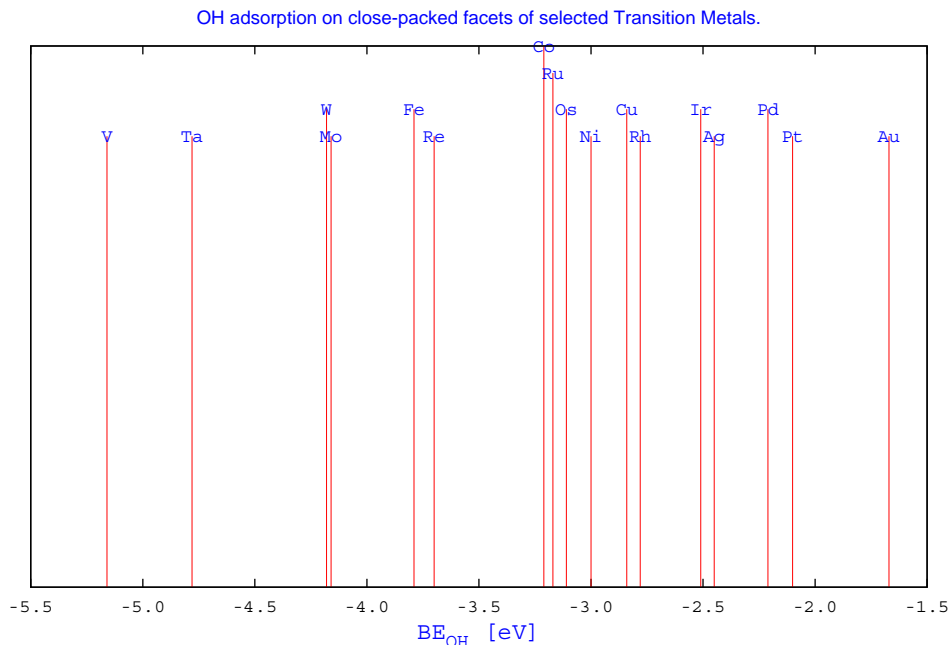
Figure 3 Strength of hydroxyl (-OH) binding on monometallic transition-metal surfaces.

Having obtained the CO BE's we moved on to analyze the trends for other species of relevance i.e. O and OH. Similar calculations were performed and the results are summarized in Figure 2 and Figure 3, respectively. For Oxygen, the BE's span a range of about 5.2 eV with Au binding the weakest (-2.74 eV) and V the strongest (-7.93 eV). The OH spectrum plot (Figure 3) indicates that a range of about 3.5 eV is spanned and again, Au binds the weakest (-1.67 eV) and V the strongest (-5.16 eV). In all cases, Vanadium binds the adsorbates strongest whereas the noble metals are weak binders. The CO spectrum (Figure 1) is distinctive in two respects; the very weak binding exhibited by Cu and the presence of a "BE gap".

3.2. Screening of potential NSA catalysts in the presence of WGS relevant adsorbates

Having obtained the BE's for CO, O and OH on this set of 17 Transition Metal surfaces we then proceeded to identify and characterize potential NSAs from the viewpoint of their LWGS activity. Before we delve into the details of our calculations a
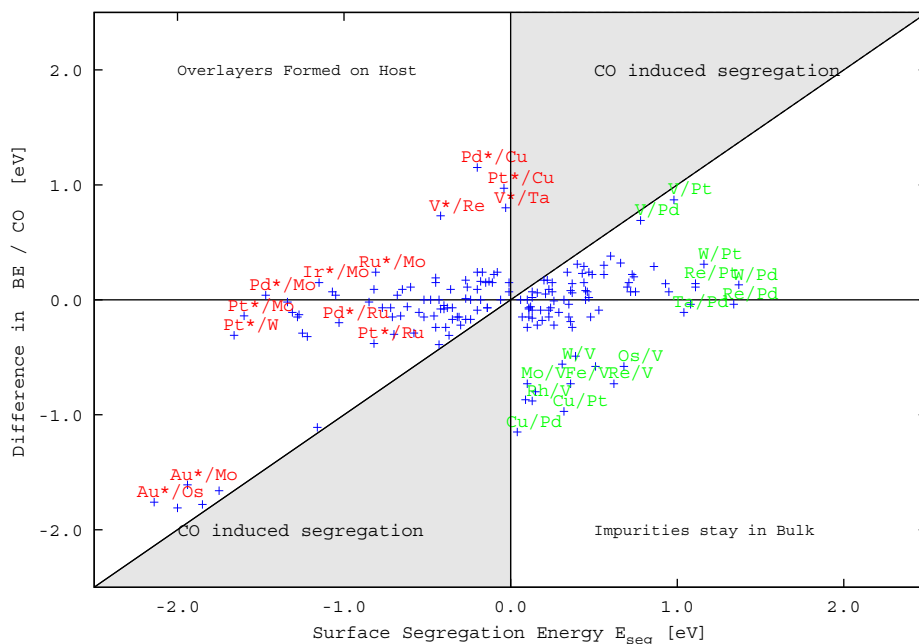
short introduction to NSAs in general and our notation and setup in particular is warranted. NSAs are alloys wherein a solute metal is present near the surface of a host metal in concentrations different from those of the bulk. As opposed to stable bulk binary alloys, for the existence of which, bulk miscibility is an essential precondition, it is possible to sustain NSAs in a stable configuration at concentrations deemed immiscible in a conventional bulk phase diagram. We focused on NSAs as promising LWGS catalysts in light of their novel electronic properties and superior catalytic behavior demonstrated by previous DFT studies in our group (pertaining to hydrogen storage, and fuel cell electrodes) and also theoretical and experimental investigations by other researchers[6-8]. Two idealized classes of NSAs are the overlayer and sandwich structures. The former is defined as a structure where the host is totally covered by a monolayer of a solute whereas the latter has a single layer of solute embedded in the next-to-surface layer of a host. In the notation that we adopt X*/Y denotes an overlayer structure with the species X (solute) in the outermost layer and the species Y (host) present in the bulk of the slab. On the other hand, the notation Y/X denotes a sandwich structure with solute Y embedded in bulk X. These features of NSA morphology are graphically illustrated in Figure 4.
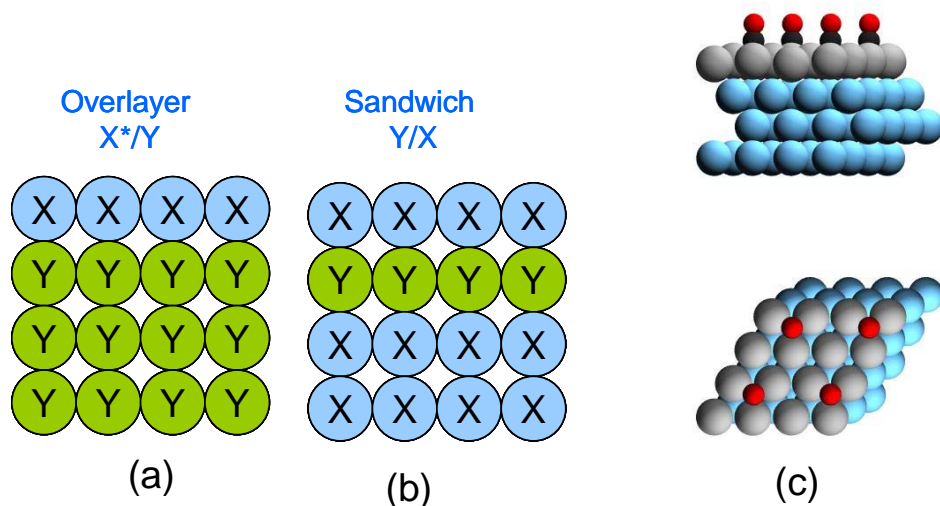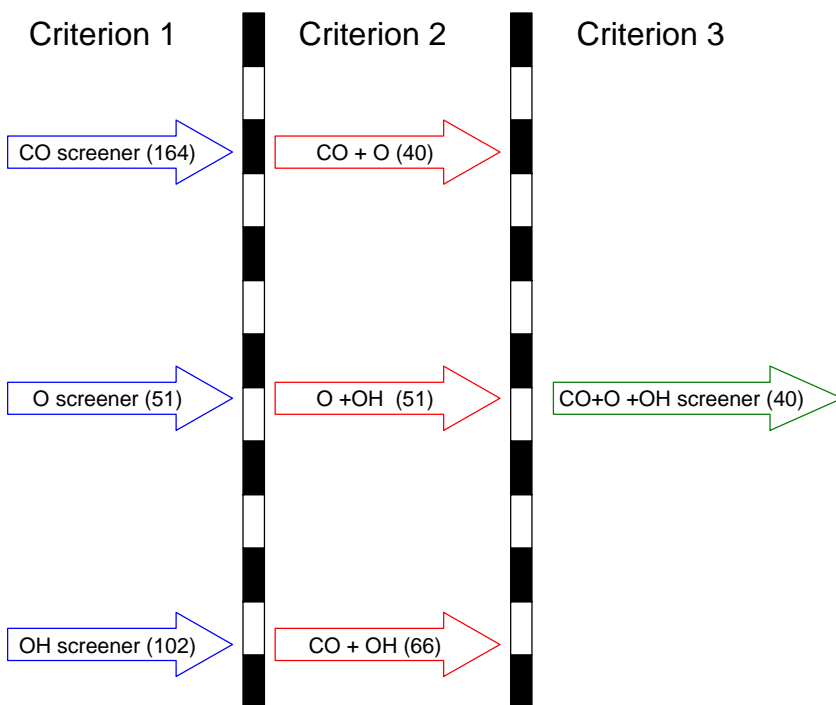

Figure 4 Schematic overview of NSA structure and notation.

(a) X*/Y Overlayer structure. X=Impurity; Y=Host. (b) Y/X Sandwich (or subsurface alloy) structure. Y=Impurity; X=Host. (c) Cross-section and top views of a 4 layer Pt*/Ru overlayer NSA with CO adsorbed at the fcc site.

Recall that our desire was to calculate the BE's of CO, O and OH on a set of NSA structures that survived the test of surface stability in the presence of these adsorbates and then based on the strength of the BE's on these candidate NSAs identify potentially promising NSA catalysts for a detailed kinetic study of H_2O activation. The stability can be estimated by using the segregation energy database for Transition Metals established by Ruban *et al.*[9] and then following the two step procedure developed by Greeley and Mavrikakis.[10]. First, the stability of the NSA is examined without reference to an adsorbate and then in a subsequent step the influence of adsorbate-induced segregation is accounted for. Thus, there are two competing factors: the segregation energy and the BE difference of the metal pair under consideration and the individual magnitudes and signs determine whether the NSA would retain its stable under vacuum configuration. The details of these screening calculations for the CO species are shown in Figure 5 which ultimately identifies a set of "survivors" when the screening criteria mentioned earlier are applied. Some representative NSAs are labeled in Figure 5, but in general any point that does not fall in the hatched region was a suitable candidate for further study. Similar plots were developed to investigate the effects of O and OH induced segregation separately but are not included in this report for the sake of brevity.

Figure 5: The "CO screener plot": Identification of NSAs stable in a CO rich environment:

Criterion 1	Criterion 2	Criterion 3
CO screener (164)	CO + O (40)	
O screener (51)	O +OH (51)	CO+O +OH screener (40)
OH screener (102)	CO + OH (66)	

**Figure 6 Employment of a cascade of screening criteria for the reduction of the set of potentially stable LWGS catalysts.**

3.3. Adsorption of CO, O and OH on NSAs (sub-surface alloys and overlayers)

It was not computationally feasible to evaluate CO, O and OH BE's on all the "survivor" NSA systems. We applied heuristics based on our past experience to select the most promising NSAs. 66 NSAs were analyzed for BE_{CO}, 43 NSAs for BE_{O} and 79 NSAs for BE_{OH}. All high symmetry sites were tested to establish the best binding sites on these facets. This set of calculations, although laborious, allows us to construct a comprehensive database of Binding Energies for CO, O and OH which is a fertile source to apply data-mining approaches for rational catalyst design. It would be cumbersome to represent the entire dataset in a plot, but Figure 7, Figure 8 and Figure 9 give an overview by plotting a sampling of the NSA systems considered. It is evident that for all the

adsorbates studied the NSAs succeed in bridging the gaps in the BE Spectra of the monometallic systems in a quasi-continuous way. At the same time, we discover some NSAs (for example: Au*/Ir, Pt*/Cu for O; Pt*/Cu for OH) that bind adsorbates weaker than any of the monometallic catalysts studied so far. This special behavior in which NSAs exhibit properties beyond the range expected on the basis of either of their constituent components is particularly noteworthy. Several NSAs bind with strength weaker than what would be expected on the basis of the binding characteristics of the constituent parent metals (e.g. Au*/Re binds O weaker than both Au and Re). Although not obvious from the Figures presented here, deeper analysis reveals that in most cases the metal exposed on the surface of the NSA exerts the primary, dominant influence on the BE while the underlying metal serves to modulate this binding strength. We identify 4 NSAs that bind CO weaker than Cu, the reference LWGS catalyst, and hence would allow a considerable reduction in the potential for CO poisoning of the catalyst.
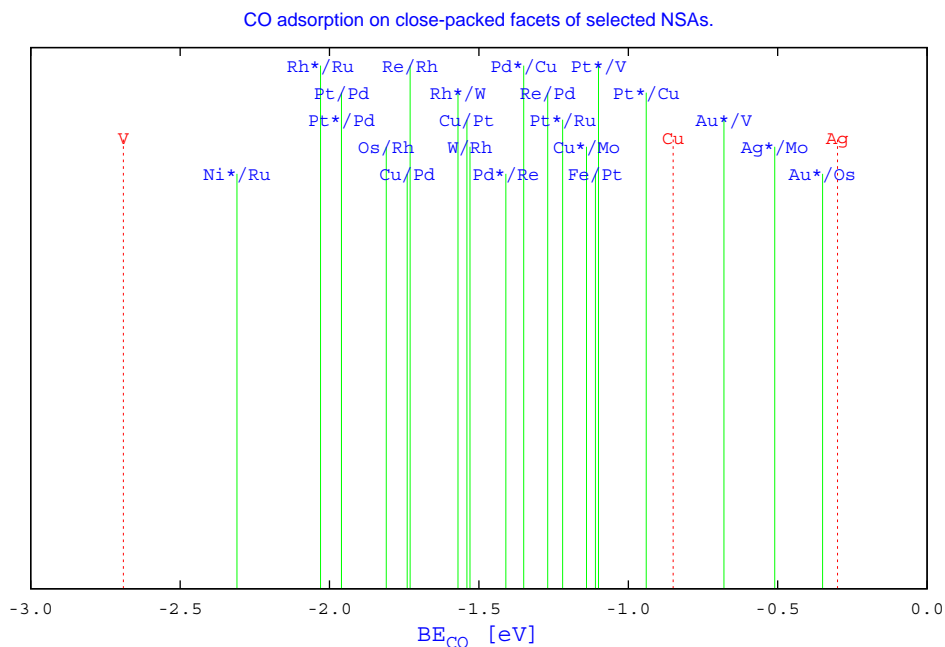
Figure 7 CO adsorption on selected NSAs (sub-surface alloys and overlayers).

O adsorption on close-packed facets of selected NSAs.
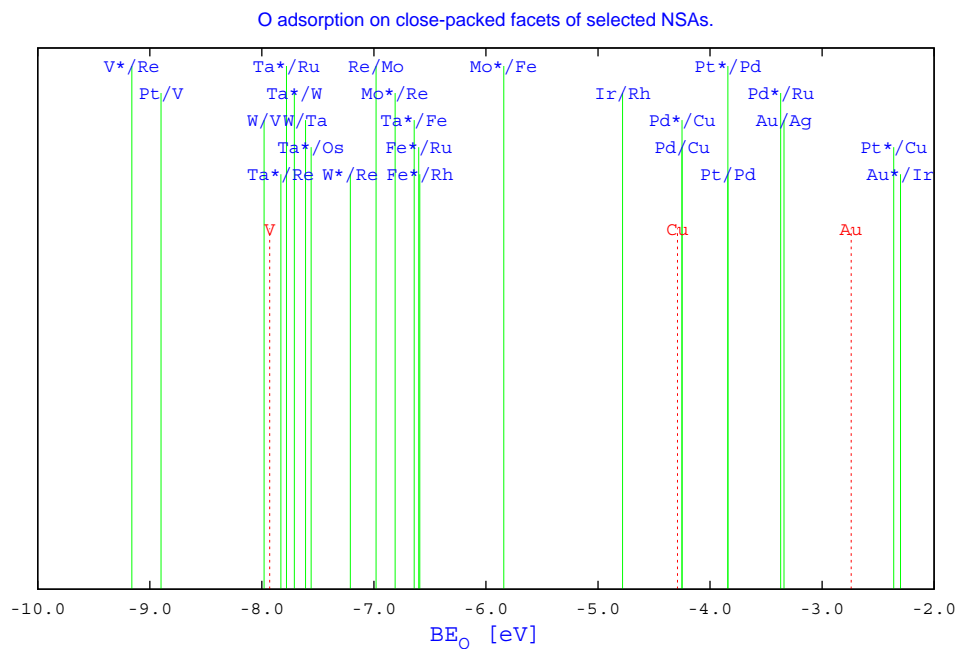
Figure 8 O adsorption on selected NSAs (sub-surface alloys and overlayers).

OH adsorption on close-packed facets of selected NSAs.
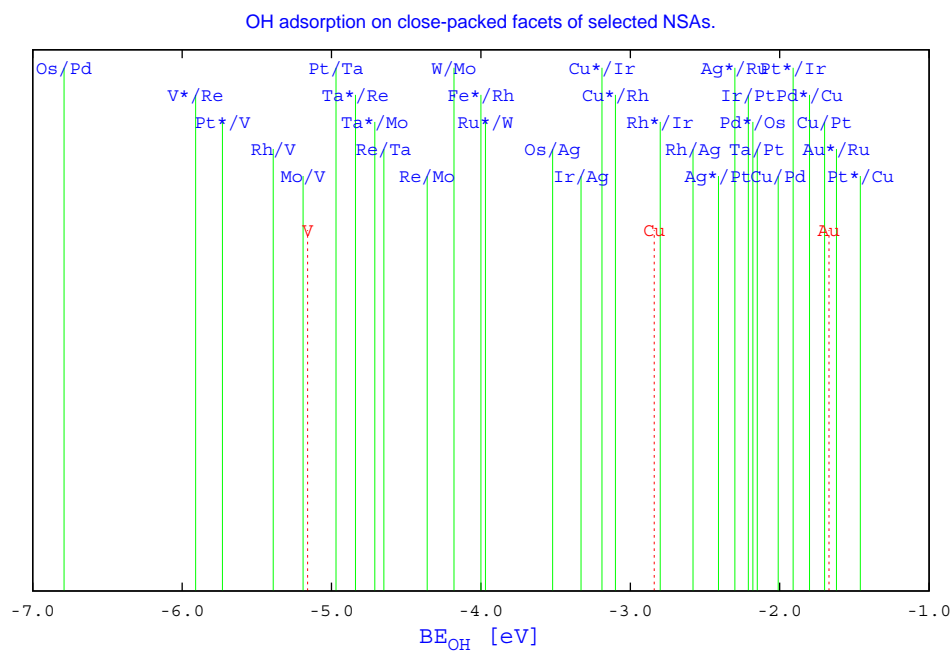
**Figure 9 OH adsorption on selected NSAs (sub-surface alloys and overlayers).**

16

3.4. Kinetic Studies for WGS on selected NSAs

Our previous studies have identified BE_{CO} as one of the two important descriptors (the other being the difficulty of H_2O activation) of LWGS activity on transition metals. Cu combines a medium strength of CO binding with a rather facile H_2O activation thereby providing an optimal balance; our endeavor was to find an NSA that can do better than Cu. We focus on NSAs that bind CO, OH and O similarly or less strongly than Cu for potentially satisfying both of the aforementioned criteria characterizing efficient LWGS catalysis. Detailed DFT studies on the thermochemistry and kinetics of H_2O activation were undertaken on promising NSAs. There were several strategies available to select this set: One possibility was to select NSAs that are "survivors" in the presence of CO, O and OH individually (Figure 6). On application of this criterion we discovered 40 systems that satisfy these requirements. Another approach would be focus on the CO, O and OH BEs and select systems that bind these species weakly and are hence likely to be better LWGS catalysts. Various such alternative screener "meshes" (similar to the ones portrayed in Figure 6) can be envisioned and dogmatic adherence to any one of these criteria would be an overly strict condition, in our opinion, and a combination of approaches was warranted.

Previous theoretical calculations for WGS had identified H_2O activation (more specifically the step $H_2O \rightarrow OH + H$) as a Rate Determining Step (RDS) on a variety of TMs. In our quest to identify catalyst that would allow facile water activation we evaluated the minimum energy pathway (MEP) and hence the activation energy for this step on a set of pure metals (Cu, Ag, Au, Pt and Ir) and promising NSA catalysts: this included the Pt-exposing overlayers Pt*/Pd, Pt*/Au, Pt*/Ir and Pt*/Ru, Pt*/Rh and also the sub-surface alloys Cu/Pt and Cu/Pd. Sulfur poisoning is a potential concern for WGS catalyst and hence the S-resistance of these catalyst was also studied: several systems were found that bind S weaker than Cu the current WGS catalyst yet provide facile H_2O activation.

Specifically, the Cu/Pt catalyst was the most promising improved WGS catalyst to be identified during this project[11]. Cu/Pt shows an enhancement of Cu concentration in the first sub-surface of the Pt host and this system has been shown to be thermodynamically stable in CO-rich environments and hence CO-induced reconstruction and segregation is not expected in this catalyst. Further, this NSA is able to easily dissociate water and binds the products of H_2O dissociation (OH + H) weaker than Cu (Figure 10). The formate intermediate (HCOO) is known to be rather stable on conventional Cu-based WGS catalysts and high coverages of this species can poison the catalyst surface and impair catalyst activity. CO is another poison implicated in WGS models, for instance on Pt. The Cu/Pt NSA that we identified binds formate weaker than Cu and CO weaker than Pt thereby making it less prone to site-blocking and poisoning by these species. Sulfur adsorption calculations indicate this catalyst possesses resistance to S-poisoning comparable to that of conventional Cu. Our assertions of the superior nature of the Cu/Pt catalyst were experimentally verified by collaborators using a variety of techniques including XPS, TPD and STM[11].
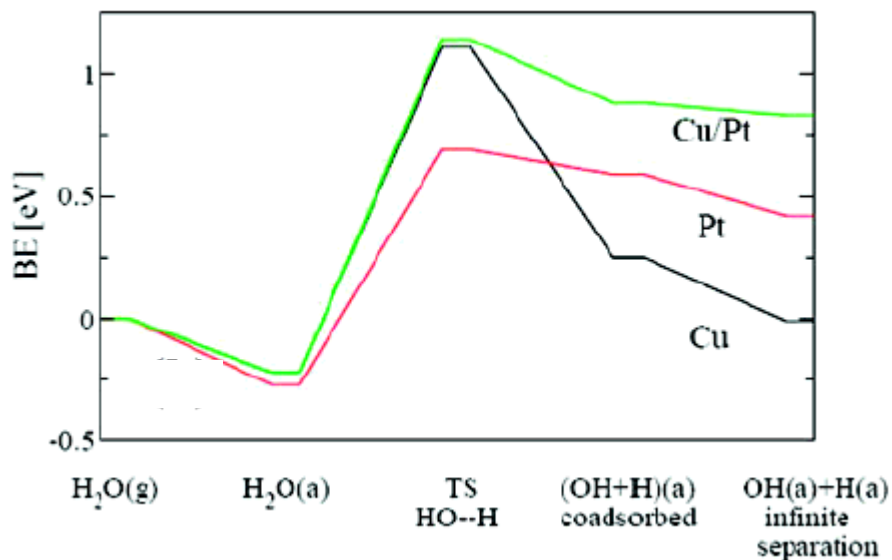
Figure 10 Potential energy surface (PES) for H_2O activation on Pt, Cu, and Cu/Pt NSA (from [11]).

18

4. Conclusions / Summary of accomplishments

The Binding Energies of WGS relevant intermediates (CO, O and OH) were evaluated on 17 catalytically relevant close-packed transition metal (TM) surfaces. A large number of bimetallic alloys can be synthesized from this set of 17 TMs and hence we employed several "screening" criteria to identify promising bimetallic NSAs deserving further study. Our main criterion was the thermodynamic stability of these NSAs, both *in vacuo* and also in the presence of the stronger-binding-adsorbates to be expected in significant coverages under typical WGS reaction conditions. A total of 40 NSAs were found to survive the strict criteria of being stable under the influence of all three species CO, O and OH. DFT calculations using the first-principles code DACAPO were performed for the adsorption of CO, O and OH on the most-stable, close-packed facets of these NSA-catalysts. The resultant BE-database was utilized for guiding the targeted discovery of novel high-activity WGS catalysts. The Cu/Pt bimetallic sub-surface alloy was identified as a promising WGS catalyst that combines the goals of high activity, stability against reconstructions and poison resistance.

5. Plans for future work

The funding for the current project got exhausted in the Fall of 2007 and hence further calculations could not be continued since. Analogous to the Cu/Pt system (that was studied in detail during this project) several other NSA-based bimetallic catalysts have been identified as potentially promising WGS catalysts. Detailed kinetic calculations for the elementary steps of WGS (with an emphasis on H_2O activation) on such a set of promising systems is warranted with the objective of expanding our set of thermodynamically-stable, highly active, poison-resistant WGS catalysts.

6. Graphical Material List / Table of Figures

7. Selected Literature References

(1)   Grenoble, D. C.; Estadt, M. M.; Ollis, D. F. *J. Catal.* **1981**, *67*, 90.
(2)   Ovensen, C. V.; Stoltze, P.; Noerskov, J. K.; Campbell, C. T. *J. Catal.* **1992**, *134*, 445.
(3)   Campbell, C. T.; Daube, K. A. *J. Catal.* **1987**, *104*, 109.
(4)   Hammer, B.; Hansen, L. B.; Nørskov, J. K. *Phys. Rev. B: Condens. Matter Mater. Phys.* **1999**, *59*, 7413.
(5)   Greeley, J.; Nørskov, J. K.; Mavrikakis, M. *Annu. Rev. Phys. Chem.* **2002**, *53*, 319.
(6)   Beutl, M.; Lesnik, J.; Rendulic, K. D.; Hirschl, R.; Eichler, A.; Kresse, G.; Hafner, J. *Chem. Phys. Lett.* **2001**, *342*, 473.
(7)   Zhou, S. G.; McIlwrath, K.; Jackson, G.; Eichhorn, B. *J. Am. Chem. Soc.* **2006**, *128*, 1780.
(8)   Lang, H.; Maldonado, S.; Stevenson, K. J.; Chandler, B. D. *J. Am. Chem. Soc.* **2004**, *126*, 12949.
(9)   Ruban, A. V.; Skriver, H. L.; Nørskov, J. K. *Phys. Rev. B* **1999**, *59*, 15990.
(10)   Greeley, J.; Mavrikakis, M. *Nat. Mater.* **2004**, *3*, 810.
(11)   Knudsen, J.; Nilekar, A. U.; Vang, R. T.; Schnadt, J.; Kunkes, E. L.; Dumesic, J. A.; Mavrikakis, M.; Besenbacher, F. *J. Am. Chem. Soc.* **2007**, *129*, 6485.

8. List of Published Journal Articles

1. **"A Cu/Pt Near-Surface Alloy for improved water-gas shift catalysis",** Knudsen, J.; Nilekar, A. U.; Vang, R. T.; Schnadt, J.; Kunkes, E. L.; Dumesic, J. A.; Mavrikakis, M.; Besenbacher, F. *J. Am. Chem. Soc.* **2007**, *129*, 6485.

9. Awards/Distinctions for the PI

1. **Editorial Board** of *Surface Science*
2. **Editorial Board** of *Annual Review of Chemical & Biomolecular Engineering*
3. **Samuel C. Johnson Distinguished Fellowship**.
4. **Visiting Professor,** Department of Chemical Engineering, Technical University of Denmark, Lyngby, Denmark (Fall 2006).
5. Featured in: **Chemical & Engineering News**, Mar. 24, 2008, Vol. 86, Issue 12, p. 40-41. (http://pubs.acs.org/isubscribe/journals/cen/86/i12/html/8612scic.html).
6. Featured in NERSC News (March 2007): http://www.nersc.gov/news/nerscnews/NERSCNews_2007_03.pdf
7. Member of the **Advising Board** for the Center for Atomic-scale Materials Design (CAMD), Department of Physics, Technical University of Denmark, Lyngby, Denmark (1/07-).

10. Students supported by this grant

Partial support for Rahul Nabar and Anand Nilekar

11. List of Acronyms and Abbreviations

LWGS	Low Temperature Water Gas Shift
WGS	Water Gas Shift
NSA	Near Surface Alloy
DFT	Density Functional Theory
BE	Binding Energy
GGA	Generalized Gradient Approximation
PW91	Perdew-Wang 91
TM	Transition Metal
RDS	Rate Determining Step
MEP	Minimum Energy Pathway
NEB	Nudged Elastic Band
XPS	X-ray photoelectron spectroscopy
TPD	Temperature Programmed Desorption
STM	Scanning Tunneling Microscopy
TS	Transition State
PES	Potential Energy Surface

A Cu/Pt Near-Surface Alloy for Water−Gas Shift Catalysis

Jan Knudsen,[†] Anand U. Nilekar,[‡] Ronnie T. Vang,[†] Joachim Schnadt,[†]
Edward L. Kunkes,[‡] James A. Dumesic,[‡] Manos Mavrikakis,*[,‡] and
Flemming Besenbacher*[,†]

*Contribution from the Interdisciplinary Nanoscience Center (iNANO) and Department of Physics
and Astronomy, University of Aarhus, DK-8000 Aarhus C, Denmark, and Department of
Chemical and Biological Engineering, University of Wisconsin−Madison,
Madison, Wisconsin 53706*

Received January 5, 2007; E-mail: manos@engr.wisc.edu; fbe@inano.dk

Abstract: The primary route to hydrogen production from fossil fuels involves the water−gas shift (WGS) reaction, and an improvement in the efficiency of WGS catalysts could therefore lead to a major leap forward in the realization of hydrogen economy. On the basis of a combination of high-resolution scanning tunneling microscopy, X-ray photoelectron spectroscopy, and density functional theory (DFT) calculations, we suggest the existence of a new thermodynamically stable Cu/Pt near-surface alloy (NSA). Temperature-programmed desorption and DFT reveal that this Cu/Pt NSA binds CO significantly more weakly than does Pt alone, thereby implying a considerable reduction in the potential for CO poisoning of the Cu/Pt NSA surface as compared to that of pure Pt. In addition, DFT calculations show that this Cu/Pt NSA is able to activate H_2O easily, which is the rate-determining step for the WGS on several metal surfaces, and, at the same time, to bind the products of that reaction and formate intermediates rather weakly, thus avoiding possible poisoning of the catalyst surface. The Cu/Pt NSA is thus a promising candidate for an improved WGS catalyst.

1. Introduction

The water−gas shift (WGS) reaction, in which carbon monoxide (CO) reacts with water (H_2O) to form carbon dioxide (CO_2) and hydrogen (H_2),[1] is used extensively in the conversion of fossil fuel to hydrogen. In particular, WGS removes residual CO from reformate hydrogen gas, which is important when hydrogen is used as a fuel for low-temperature fuel cells; the performance of such fuel cells is very sensitive to CO impurities because of CO poisoning of the Pt-based anode.[2−4]

The WGS reaction is slightly exothermic (∼40 kJ/mol), and therefore low reaction temperatures push the equilibrium toward hydrogen production, while high reaction temperatures provide faster kinetics. To deal with these two opposing temperature effects, large-scale industrial plants often use a two-step WGS reactor in which the feed gas is led through a high-temperature WGS reactor and then a low-temperature recator.[5] However, such a two-step process is not a viable solution for small-scale applications such as on-board reformers in hydrogen fuel cell-powered automobiles. Consequently, it is very important to develop new WGS catalysts with high activity at lower

temperatures than the presently used low-temperature Cu-based WGS catalysts.

Transition metal alloys are very often superior to pure transition metals as the active materials in heterogeneous catalysis.[6] During the past century, the development of alloy catalysts has almost exclusively been accomplished by trial and error. Recent advances in both experimental and theoretical methods, however, have facilitated the development of new and improved alloy catalysts based on fundamental surface science and first-principles studies.[7−10] These advances continue to pave the way for a new era in which promising catalysts may be identified directly from first principles.[8,11−13]

Here, we report on a novel Cu/Pt near-surface alloy (NSA) with an enhanced Cu concentration in the first subsurface layer of the Pt host, which is shown to be a promising candidate for an improved low-temperature WGS catalyst. From an interplay of scanning tunneling microscopy (STM), X-ray photoelectron

---

[†] University of Aarhus.
[‡] University of Wisconsin−Madison.
(1) Ovesen, C. V.; Stoltze, P.; Norskov, J. K.; Campbell, C. T. *J. Catal.* **1992**, *134*, 445−468.
(2) *Handbook of Fuel Cells: Fundamentals, Technology, Applications*; Wiley: West Sussex, UK, 2003.
(3) Oetjen, H. F.; Schmidt, V. M.; Stimming, U.; Trila, F. *J. Electrochem. Soc.* **1996**, *143*, 3838−3842.
(4) Greeley, J.; Mavrikakis, M. *Catal. Today* **2006**, *111*, 52−58.
(5) Somorjai, G. *Introduction to Surface Chemistry and Catalysis*; John Wiley & Sons: New York, 1994.

(6) Sinfelt, J. *Bimetallic Catalysts: Discoveries, Concepts and Applications*; Wiley: New York, 1983.
(7) Besenbacher, F.; Chorkendorff, I.; Clausen, B. S.; Hammer, B.; Molenbroek, A. M.; Norskov, J. K.; Stensgaard, I. *Science* **1998**, *279*, 1913−1915.
(8) Greeley, J.; Mavrikakis, M. *Nat. Mater.* **2004**, *3*, 810−815.
(9) Vang, R. T.; Honkala, K.; Dahl, S.; Vestergaard, E. K.; Schnadt, J.; Laegsgaard, E.; Clausen, B. S.; Norskov, J. K.; Besenbacher, F. *Nat. Mater.* **2005**, *4*, 160−162.
(10) Jacobsen, C. J. H.; Dahl, S.; Clausen, B. S.; Bahn, S.; Logadottir, A.; Norskov, J. K. *J. Am. Chem. Soc.* **2001**, *123*, 8404−8405.
(11) Zhang, J. L.; Vukmirovic, M. B.; Xu, Y.; Mavrikakis, M.; Adzic, R. R. *Angew. Chem., Int. Ed.* **2005**, *44*, 2132−2135.
(12) Zhang, J. L.; Vukmirovic, M. B.; Sasaki, K.; Nilekar, A. U.; Mavrikakis, M.; Adzic, R. R. *J. Am. Chem. Soc.* **2005**, *127*, 12480−12481.
(13) Greeley, J.; Jaramillo, T. F.; Bonde, J.; Chorkendorff, I. B.; Norskov, J. K. *Nat. Mater.* **2006**, *5*, 909−913.
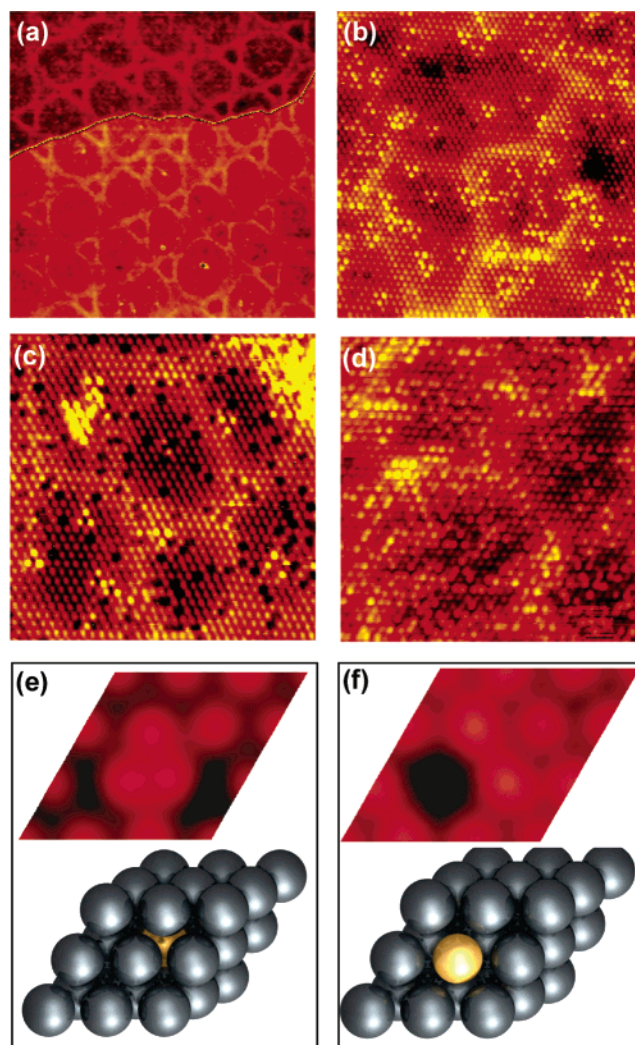
spectroscopy (XPS), and density functional theory (DFT) calculations, we show that a thermodynamically stable Cu/Pt NSA, with Cu preferentially located in the first subsurface layer, is formed upon evaporation of 1 monolayer (ML) of Cu onto Pt(111) at 800 K. Temperature-programmed desorption (TPD) and DFT studies show that the potential for CO poisoning of the Cu/Pt NSA is reduced compared to that of pure Pt. Finally, we use DFT to analyze trends in catalytic activation of water, which is the rate-determining step for the WGS on several metal surfaces, and the binding of formate, a common spectator species that blocks sites on Cu WGS catalysts. By combining these results, we propose that the Cu/Pt(111) NSA possesses a higher WGS activity than the pure Cu(111) surface of the industrially used WGS catalyst.

2. Methods

The STM experiments were performed in an ultra-high-vacuum system with a base pressure of $\sim 10^{-10}$ Torr, equipped with the home-built Aarhus STM.[14] A Pt(111) crystal was cleaned with cycles of Ar ion sputtering (1.0 keV, 10 min) followed by annealing to 1000 K for 3 min. These cycles were repeated until no contamination of the crystal could be detected with the STM. Cu was deposited either by a home-built evaporator consisting of a piece of Cu placed in a resistively heated tungsten crucible or with a mini e-beam evaporator (Oxford Applied Research). Both evaporators were calibrated from STM pictures of Cu evaporated onto Pt(111) at room temperature. All XPS measurements of Cu 3s were performed at the SX700 beamline located at the Aarhus Storage Ring in Denmark (ASTRID), with $h\nu = 205$ eV in normal emission. A fixed 100 mm mean radius analyzer (VG-CLAM2) was used in all experiments. The TPD measurements were obtained using a Balzers quadrupole mass spectrometer, after the crystal was exposed to 10 L of CO at 166 K, and with a heating rate of 2 K/s.

The self-consistent DFT calculations were carried out using the DACAPO[15,16] total-energy code with ultrasoft pseudopotentials, plane waves with kinetic energies of up to 25 Ry, and 6 or 18 k-points in the first Brillouin zone for (111) facets of four-layer metal slabs with 3×3 and 2×2 surface unit cells, respectively. The equivalent of five layers of vacuum was used to separate periodic images of metal slabs in the z-direction of the unit cell. Adsorption is allowed on only one of the two exposed surfaces, and the electrostatic potential is adjusted accordingly.[17,18] All CO and formate (HCOO) binding energy calculations were performed at a coverage of 1/9 ML on a 3×3 surface unit cell, whereas a 2×2 unit cell was used for the calculation of the activation energy barrier for H_2O dissociation. Ionic cores were described by ultrasoft pseudopotentials,[19] and the Kohn–Sham one-electron valence states were expanded in a basis of plane waves with kinetic energy below 25 Ry. The exchange-correlation energy and potential were described self-consistently within the generalized gradient approximation (GGA-PW91).[20,21] The self-consistent PW91 density was determined by iterative diagonalization of the Kohn–Sham Hamiltonian, Fermi population of the Kohn–Sham states ($k_B T = 0.1$ eV), and Pulay mixing of the resulting electronic density.[22] All total energies have been extrapolated to $k_B T = 0$ eV. Zero-point energy effects were not considered in the reported results. Unless otherwise specified, all

(14) Laegsgaard, E.; Besenbacher, F.; Mortensen, K.; Stensgaard, I. *J. Microsc. (Oxford)* **1988**, *152*, 663–669.
(15) Hammer, B.; Hansen, L. B.; Nørskov, J. K. *Phys. Rev. B* **1999**, *59*, 7413–7421.
(16) Greeley, J.; Nørskov, J. K.; Mavrikakis, M. *Annu. Rev. Phys. Chem.* **2002**, *53*, 319–348.
(17) Neugebauer, J.; Scheffler, M. *Phys. Rev. B* **1992**, *46*, 16067–16080.
(18) Bengtsson, L. *Phys. Rev. B* **1999**, *59*, 12301–12304.
(19) Vanderbilt, D. *Phys. Rev. B* **1990**, *41*, 7892–7895.
(20) Perdew, J. P.; Chevary, J. A.; Vosko, S. H.; Jackson, K. A.; Pederson, M. R.; Singh, D. J.; Fiolhais, C. *Phys. Rev. B* **1992**, *46*, 6671–6687.
(21) White, J. A.; Bird, D. M. *Phys. Rev. B* **1994**, *50*, 4954–4957.
(22) Kresse, G.; Furthmuller, J. *Comput. Mater. Sci.* **1996**, *6*, 15–50.

Figure 1. (a–d) STM images of Cu/Pt(111) surface alloys. (a,b) Surface prepared by evaporation of 1 ML of Cu onto Pt(111) at 800 K (image sizes are 631 × 631 Å² and 132 × 132 Å², respectively). (c) Surface prepared by the evaporation of 1 ML of Cu onto Pt(111) followed by 1 ML of Pt at room temperature (100 × 100 Å²). (d) The surface in (c) after postannealing at 773 K (100 × 100 Å²). (e,f) Simulated STM images of a Cu atom (gold spheres) in the first subsurface layer (e) or in the topmost layer (f) of a Pt(111) substrate (gray spheres) within the framework of a 3 × 3 surface unit cell.

degrees of freedom for the top two layers of slab atoms and for all adsorbate atoms were relaxed. Transition states for H_2O dissociation were located with the "climbing-image nudged elastic band" method.[23]

3. Results and Discussion

When Cu was evaporated onto a Pt(111) crystal, the STM images clearly indicated the formation of an NSA.[8] In particular, Figure 1a shows an STM image of a Pt(111) surface after evaporation of 1 ML of Cu at a substrate temperature of 800 K. The surface displays a network of bright rings ordered in a nonperfect hexagonal symmetry with a periodicity of ~ 100 Å. These bright lines are speculated to be stress-induced boundaries between atoms sitting in face-centered cubic (fcc) and hexagonal close-packed (hcp) sites.[24,25] Atomically resolved images (Figure

(23) Henkelman, G.; Jónsson, H. *J. Chem. Phys.* **2000**, *113*, 9978–9985.
(24) Holst, B.; Nohlen, M.; Wandelt, K.; Allison, W. *Surf. Sci.* **1997**, *377*, 891–894.
(25) Holst, B.; Nohlen, M.; Wandelt, K.; Allison, W. *Phys. Rev. B* **1998**, *58*, R10195–R10198.

1b) reveal that the surface atoms appear with different corrugations in the STM images, which serves as a clear indication of NSA formation. In the topmost surface layer, we did not find any dislocations visible to the STM. Therefore, we conclude that the bright lines observed in the STM images are related to subsurface atoms changing between stacking of fcc and hcp sites.

A ring structure very similar to the one described above was observed when we evaporated 1 ML of Cu onto Pt(111), followed by evaporation of 1 ML of Pt at room temperature, where both Cu and Pt grow as adlayers. As can be seen in Figure 1c, similar bright lines show up in the STM images of this "sandwich" structure. However, some atoms in the topmost layer are imaged as depressions, which we did not observe in the original ring structure. These dark spots disappear upon annealing to 773 K (Figure 1d), in which case we end up with a structure almost identical to the ring structure of Figure 1b.

The wave functions derived from DFT calculations were used to calculate STM images[26] by employing the Tersoff–Hamann approach.[27] These calculations were performed for a number of configurations with Cu located on the surface and/or subsurface of Pt(111). The simulated STM image shown in Figure 1e represents a single Cu atom in the second layer of the Pt(111) slab; this image is in qualitatively good agreement with the trimers of bright atoms observed by STM between the rings in Figure 1b. The simulated STM image of a surface Cu atom in a Pt(111) substrate (Figure 1f) shows a distinct depression, which strongly suggests that the dark spots in the sandwich structure are Cu atoms incorporated in the topmost layer. These depressions are not observed in the ring structure, and we therefore conclude that evaporation of 1 ML of Cu onto Pt(111) at 800 K leads to the formation of NSA without Cu atoms in the surface layer.

To further investigate the formation of the subsurface Cu/Pt alloy, we used DFT calculations to determine the thermodynamics and energetic aspects of its formation kinetics. From calculations on a 3 × 3 surface unit cell of a seven-layer Pt-(111) slab, we found that the activation energy barrier for both Pt vacancy formation in Pt(111) and Cu adatom diffusion from the surface of Pt(111) into a Pt vacancy in Pt(111) is less than 3 eV. Barriers of this magnitude can be surmounted at 800 K, the sample temperature during the original Cu deposition, and thus we expect a structure in thermodynamic equilibrium. We analyzed the relative stability of Cu atoms in various layers of the seven-layer Pt(111) slab, now allowing for relaxation of the top five layers. By replacing one or two of the Pt atoms in the slab with Cu atoms, either in the top (i.e., surface) layer or in the second, third, or fourth layer of the slab, we were able to determine the relative energetics as a function of Cu coverage (1/4 or 1/2 ML, respectively). We found that 1/4 ML of Cu is more stable when located in the second, third, or fourth layer of the slab by 0.48, 0.34, or 0.35 eV, respectively, than when Cu is located in the surface layer. Furthermore, these trends in the relative energetics of Cu in Pt(111) remain practically invariant when the Cu coverage is increased to 1/2 ML or when a Pt(100) facet is considered instead of the Pt(111) facet. Studies of Cu on/in facets of Pt other than the (111) facet may be

relevant to realistic catalyst nanoparticles, naturally exposing a mixture of crystallographic facets. In all cases, the relative stability of Cu in the third and fourth layers of the Pt slab appears to be converged to what we consider to be the stability of Cu in bulk Pt. These results show that a significant driving force causes Cu to diffuse into the Pt slab rather than staying in the surface layer, and that the thermodynamics of Cu–Pt alloy dictate a preferential occupation of sites within the first subsurface layer of Pt(111).

This conclusion was verified by XPS measurements, which showed a 70% attenuation of the Cu 3s peak when an overlayer of Cu on Pt(111) was flashed to 800 K, while the peak intensity was not attenuated any further when the sample was kept at 800 K for longer periods.

Finally, our DFT results for Cu on/in Pt(100) indicate trends similar to those established above for Pt(111), in terms of both the thermodynamics and kinetics of the subsurface alloy formation. If anything, the migration of Cu to the subsurface of Pt becomes even easier through the more open (100) facet.

A depth profile of Cu in the Pt(111) host can be obtained from the DFT-calculated stabilization energies of Cu in different layers and the XPS data discussed above. The Cu 3s intensity of the subsurface alloy, I, relative to the intensity of the overlayer, I_0, can be expressed as the following sum, if it is assumed that the Cu atoms are distributed in a finite number of layers, N, close to the surface:

$$\frac{I}{I_0} = \sum_{i=1}^{N} c_i \exp\left(-\frac{(i-1)d}{\mu}\right)$$

Here, c_i is the concentration of Cu in layer i, μ is the inelastic mean free path of the electron in Pt(111), and d is the interlayer distance in Pt(111) since the amount of Cu in the Pt(111) host is relatively low. The concentration of Cu atoms in the surface layer is observed to be zero in the STM, as discussed above, and c_1 is therefore equal to zero. The DFT calculations show that the relative stability of Cu converges to the bulk value in the third layer, and c_i is therefore assumed to be constant for $i \geq 3$. From a Boltzman distribution, we can determine the relative Cu concentration in the second layer (c_2) with respect to the bulk value (c_{bulk}):

$$\frac{c_2(Cu)}{c_{bulk}(Cu)} = \exp\left(\frac{E_2 - E_{bulk}}{kT}\right)$$

$$= \exp\left(\frac{0.48\ eV - 0.35\ eV}{(8.62 \times 10^{-5}\ eV/K) \times 800\ K}\right) = 6.6$$

Finally, the sum can be rewritten as

$$\frac{I}{I_0} = 0.30 = c_2 \exp\left(\frac{-d}{\mu}\right) + \frac{c_2}{6.6} \sum_{i=3}^{N} \exp\left(\frac{-(i-1)d}{\mu}\right)$$

This equation is solved under the constraint that the total amount of Cu is fixed to 1 ML. The best agreement with the experimentally observed damping is obtained with 0.4 ML of Cu in the second layer and 0.06 ML of Cu in layers 3−11.

Having discussed the atomic-scale structure of the Cu/Pt NSA, we now turn our attention to its WGS reactivity. First, we use DFT calculations and TPD experiments to probe the strength

(26) Bollinger, M. V.; Lauritsen, J. V.; Jacobsen, K. W.; Norskov, J. K.; Helveg, S.; Besenbacher, F. *Phys. Rev. Lett.* **2001**, *87*, 196803.
(27) Tersoff, J.; Hamann, D. R. *Phys. Rev. B* **1985**, *31*, 805−813.
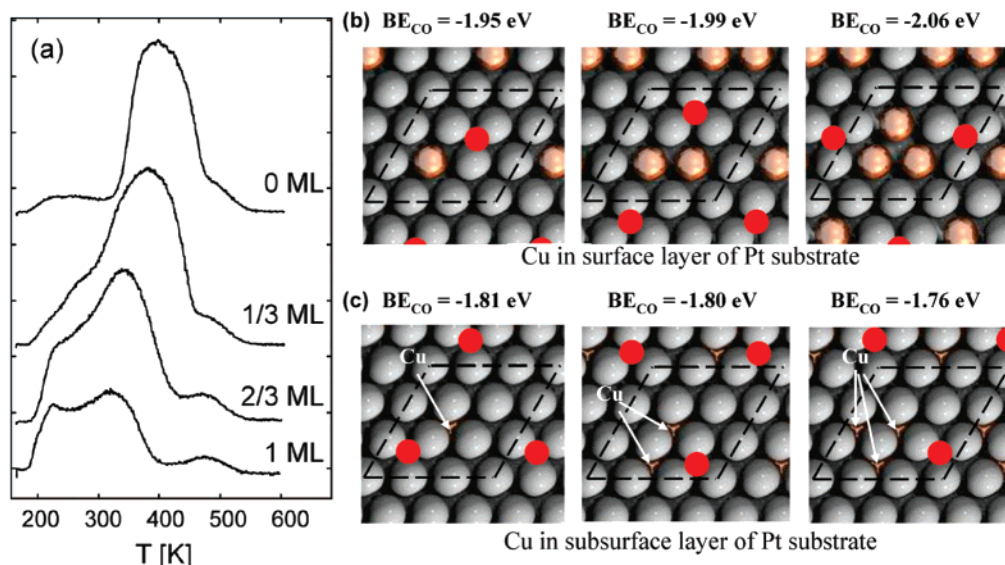
Figure 2. (a) Series of CO TPD spectra for Cu/Pt(111) surface alloys with varying amounts of Cu after exposure of 10 L of CO at 166 K. (b,c) Binding energies for 1/9 ML of CO on different Cu/Pt surface and subsurface alloys, respectively, as calculated from a 3 × 3 surface unit cell (for comparison, BE_{CO} on pure Pt(111) = −1.82 eV). Gray and gold spheres represent Pt and Cu atoms, respectively. In each of the panels (b) and (c), three top views of the respective alloy slabs are shown: left, 1/9ML of Cu; middle, 2/9 ML of Cu; right, 3/9 ML of Cu. The surface unit cell is sketched in each image, with the most favored CO adsorption site shown with a red circle. In panel (c), arrows show the location of the subsurface Cu atoms.

of the interaction between CO and the Cu/Pt NSA; the stronger the interaction, the more likely the site-blocking by CO would be. In particular, we calculated the binding energy ($E_b = E_{total} - E_{substrate} - E_{gas-phase\ adsorbate}$) of CO on pure Pt(111) and on Cu/Pt(111) NSAs with varying concentrations of Cu in the surface and subsurface layers at a CO coverage of 1/9 ML. For reference, the binding energy of CO on Pt(111) is found to be −1.82 eV. It should be noted that, although DFT methods are unable to capture the most stable CO adsorption site on Pt-(111),[28] here we focus only on the trends in CO binding energies on different surfaces, and these relative trends should not be affected by that inability. When the Cu coverage for the Cu overlayer structures was increased from 1/9 to 1/3 ML, an increase in the magnitude of the binding energy of CO in the most preferred site (fcc site formed by three Pt atoms) was calculated. The CO binding energies in these cases amount to −1.95 eV for 1/9 ML of Cu and −2.06 eV for 1/3 ML of Cu (see Figure 2b). For the Cu subsurface alloys of Pt(111), we observe exactly the opposite behavior. As the Cu concentration in the second layer of the slab is increased from 1/9 ML to 1/3 ML, the magnitude of the CO binding energy on the most preferred surface site decreases from −1.81 to −1.76 eV, as shown in Figure 2c. As the amount of Cu in the subsurface layer is further increased to 1 ML, the CO binding is decreased by 0.33 eV, to −1.48 eV. CO binding is significantly weaker on a full ML of Cu overlayer on top of Pt(111) (−1.16 eV) as compared to the different structures considered above, but it is important to remember that this structure is not thermodynamically stable because Cu is clearly more stable in subsurface layers.

The trends in CO binding energies as predicted by DFT were investigated experimentally by performing TPD measurements on various Cu/Pt(111) structures. A series of CO TPD spectra from Cu/Pt(111) subsurface alloys, prepared by evaporating

varying amounts of Cu onto Pt(111) at 800 K, is depicted in Figure 2a. The TPD spectrum from the pure Pt(111) surface has a broad but distinct peak with a maximum intensity at 400 K and a small, high-temperature shoulder, which is ascribed to defects such as step edges.[29] When the amounts of Cu alloyed into Pt(111) are increased, the main TPD peak shifts toward lower temperatures, which shows that the Cu atoms weaken the interaction between the surface alloy and CO. This trend in CO binding energy as a function of Cu coverage is exactly what is found in the DFT calculations for the Cu/Pt(111) subsurface alloys, but not for the surface alloys. Therefore, the combination of DFT and TPD shows that the thermodynamically stable Cu/Pt NSA binds CO significantly more weakly than Pt(111) does, thereby implying a considerable enhancement of CO-tolerance of the Cu/Pt NSA surface as compared to that of pure Pt.

Detailed studies of the low-temperature WGS reaction mechanism on a number of late transition metals[30] suggest that H_2O activation, and in particular its first step ($H_2O \rightarrow OH + H$), is the rate-determining step for several of these metals. This includes Cu, the current catalyst of choice for industrial WGS applications,[31] and Pt. Accordingly, we have studied the minimum energy path of water activation on three different model surfaces, Cu(111), Pt(111), and a full ML of Cu in the first subsurface layer of a Pt(111) slab. As shown above, Cu preferentially segregates into the first subsurface layer of Pt(111) without necessarily reaching a full ML coverage in that layer. However, previous calculations on NSAs[8] showed that positive kinetic effects (such as decreased activation energies) observed at full ML subsurface alloys tend to be preserved by-and-large, even in the case of less than a ML of solute coverage in the subsurface layer. This finding reflects the importance of local

(28) Feibelman, P.; Hammer, B.; Nørskov, J.; Wagner, F.; Scheffler, M.; Stumpf, R.; Watwe, R.; Dumesic, J. *J. Phys. Chem. B* **2001**, *105*, 4018−4025.

(29) Pedersen, M. O.; Helveg, S.; Ruban, A.; Stensgaard, I.; Laegsgaard, E.; Norskov, J. K.; Besenbacher, F. *Surf. Sci.* **1999**, *426*, 395−409.
(30) Gokhale, A. A. Ph.D. thesis, University of Wisconsin−Madison, 2005.
(31) Chorkendorff, I.; Niemantsverdriet, J. W. *Concepts of Modern Catalysis and Kinetics*; Wiley-VCH: Weinheim, 2003.
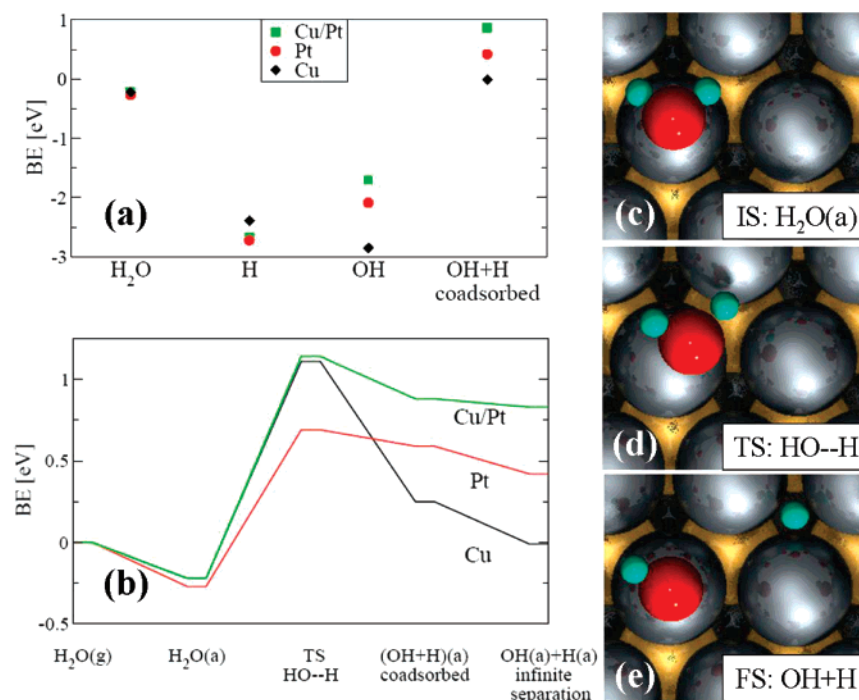
Figure 3. (a) Binding energies (BE) of H_2O (ref $H_2O(g)$), H (ref H(g)), OH (ref OH(g)), and coadsorbed OH + H (ref $H_2O(g)$) on Cu(111), Pt(111), and Cu/Pt(111), all calculated on a 2 × 2 unit cell, for the energetically preferred states. (b) Potential energy diagram for the activation of H_2O on Cu/Pt(111) subsurface alloy, Cu(111), and Pt(111) with $H_2O(g)$ as the zero of the energy axis. (c−e) Top view of DFT-calculated structures for the initial (IS), transition (TS), and final (FS) states of H_2O activation on the Cu/Pt(111) subsurface alloy. Red, green, gray, and gold spheres represent O, H, Pt, and Cu atoms, respectively.

electronic structure in determining specific site reactivity. Thus, by choosing a high-symmetry, full ML Cu/Pt subsurface alloy, we can examine the influence of subsurface Cu on the reactivity of the Pt surface.

The binding energies at their preferred adsorption sites of H, OH, and H_2O on all three surfaces are shown in Figure 3a. We find that, in the 2 × 2 unit cell, H and OH occupy three-fold fcc sites on all three surfaces, with the exception of OH occupying top/bridge site on the pure Pt(111) surface. In the relevant coadsorbed states, representing the final state of H_2O activation, OH and H occupy top−fcc, fcc−fcc, and top−top combinations of sites on Cu/Pt(111), Cu(111), and Pt(111), respectively. The variation in the binding energy of H on these three surfaces is small (within 0.20 eV) as compared to the corresponding variation of the OH binding energy (1.15 eV). OH binds to Cu/Pt(111) with −1.70 eV, significantly weaker than on Cu(111) and Pt(111), to which it binds with −2.85 and −2.09 eV, respectively. H_2O interacts rather weakly with all three surfaces.

Following the trend in relative stability of adsorbed OH discussed above, the coadsorbed state of the products for the $H_2O \rightarrow OH + H$ step is most stable on Cu(111), followed by Pt(111) and then by Cu/Pt(111). A significant repulsion between coadsorbed OH and H calculated on the Cu(111) surface tends to stabilize the products of this reaction even further when OH and H can diffuse away from each other (compare the coadsorbed state and infinite separation state, as shown in Figure 3b). However, this is not the case on the other two surfaces, where the repulsive interaction between coadsorbed OH and H is only minimal. Figure 3b shows that the activation energy barrier for the $H_2O \rightarrow OH + H$ elementary step is the smallest on Pt(111), a modest 0.96 eV, whereas the corresponding barriers on Cu(111) and Cu/Pt(111) subsurface alloy are 1.34

and 1.36 eV, respectively. Top views of the initial, transition, and final states for this elementary step on the Cu/Pt surface are shown in Figure 3c−e. We note in passing that, although Cu-(111) binds OH(a) + H(a) more strongly than Pt(111) does, the latter appears to break the H−OH bond more easily than the former. The H−OH bond-breaking steps on Cu(111) and on the subsurface alloy Cu/Pt(111) have similar transition state (TS) energies. However, the NSA offers a considerable advantage, namely that the product of the reaction, OH, is bound much more weakly than OH on Cu(111), and therefore the potential for catalyst poisoning by that intermediate is reduced on the Cu/Pt alloy. The activation energy barrier for H_2O activation on Pt(111) is the smallest of those on all three surfaces studied (see Figure 3). Nevertheless, CO poisoning of pure Pt catalysts is the main reason for the low WGS activity observed on those catalysts.

Formate intermediate (HCOO) is another key WGS reaction intermediate known to be rather stable on Cu surfaces.[30] In particular, formate species occupy a large fraction of Cu surface sites under typical WGS conditions, thereby blocking them from participating in active WGS chemistry. Our calculations show that, following the relative binding energy trends established for OH between Cu and Cu/Pt NSA, formate is also destabilized on the Cu/Pt(111) NSA by ca. 0.9 eV at 1/9 ML coverage, compared to its binding on pure Cu(111). This finding suggests that Cu/Pt NSA catalysts should be able to activate H_2O as easily as Cu and, at the same time, be less prone to CO poisoning than pure Pt and more resistant to site blocking by formate than pure Cu surfaces would be.

On the basis of our first-principles calculations, we therefore predict that the reduced poisoning by CO and formate on the Cu/Pt subsurface alloy should make this NSA a very promising and active WGS catalyst. We note here that, as for H_2 dissociation, an NSA is indeed able to activate the H−OH bond

in H_2O relatively easily while binding the products of the reaction rather weakly.[8] Furthermore, the NSAs of Cu/Pt are found to be stable in CO-rich environments, and CO-induced segregation is therefore not expected.[13]

We have thus shown that the stable Cu/Pt NSA is able to activate H_2O (a very common reactant) easily and, at the same time, to bind the products of that reaction and formate intermediates rather weakly, thus avoiding possible poisoning of the catalyst surface. Interestingly, we would like to mention that recently Zhou et al.[32] reported an anomalously high catalytic activity of CuPt core−shell nanoparticles for the NO reduction reaction. After a thorough characterization of their nanoparticles, those authors concluded that the most active phase of their catalysts had Cu preferentially located in the subsurface layers of the Pt nanoparticles.

4. Conclusions

By using a combination of experimental and theoretical model studies, we identified a novel Cu/Pt near-surface alloy which was shown to be a promising candidate for an improved low-temperature WGS catalyst. Such an NSA catalyst might be extremely relevant to hydrogen economy-related catalysis and

practice. Advanced nanosynthesis techniques, including electrochemical deposition of metals on metals,[33] dendrimer-based approaches,[34] and atomic layer deposition[35] techniques, all hold a very strong promise for large-scale preparation of NSA catalysts with superior performance when compared to monometallic or bulk alloy catalysts. Such emerging catalyst nanosynthesis techniques can enable the large-scale preparation of improved catalysts, and we hope that the present study will inspire such advances.

(32) Zhou, S. H.; Varughese, B.; Eichhorn, B.; Jackson, G.; McIlwrath, K. *Angew. Chem., Int. Ed.* **2005**, *44*, 4539−4543.

(33) Brankovic, S. R.; Wang, J. X.; Adzic, R. R. *Surf. Sci.* **2001**, *474*, L173−L179.
(34) Ye, H. C.; Crooks, R. M. *J. Am. Chem. Soc.* **2005**, *127*, 4930−4934.
(35) Lim, B. S.; Rahtu, A.; Gordon, R. G. *Nat. Mater.* **2003**, *2*, 749−754.